Experimental Results for 3D Bipedal Robot Walking Based On Systematic Optimization of Virtual Constraints

Brian G. Buss[1], Kaveh Akbari Hamed[2], Brent A. Griffin[1], and Jessy W. Grizzle[1]

Abstract— **Feedback control laws which create asymptotically stable periodic orbits for hybrid systems are an effective means for realizing dynamic legged locomotion in bipedal robots. To address the challenge of *designing* such control laws, we recently introduced a method to systematically select a stabilizing feedback control law from a parameterized family of feedback laws by solving an offline optimization problem. The method has been used elsewhere to design a stable gait based on virtual constraints, and its potential effectiveness was illustrated via simulation results. In this paper, we present the first experimental demonstration of a controller designed using this new offline optimization method. The new controller is compared with a nominal controller in experiments on MARLO, a 3D point-foot bipedal robot. Compared to the nominal controller, the optimized controller leads to improved lateral control and longer sustained walking.**

I. INTRODUCTION

This paper presents experimental implementation of a novel method to exponentially stabilize periodic orbits in hybrid systems [1], [2]. The experimental apparatus is the underactuated 3D bipedal robot shown in Fig. 1, called MARLO [3], [4]. The robot is equipped with point feet for the study of mechanical bipedal walking that allows a natural rolling motion at the "feet," as opposed to the flat-footed walking used by the vast majority of bipedal robots today. Indeed, all of the bipedal robots participating in the June 2015 DARPA Robotics Challenge relied on flat-footed walking [5].

The method of Poincaré sections is the primary tool for analyzing the stability of periodic orbits in a hybrid system, such as those that arise in bipedal locomotion [6]–[8], though Lyapunov-based techniques are being developed [9]. Under mild technical conditions, a necessary and sufficient condition for a periodic orbit in the hybrid model to be exponentially stable is that the Jacobian of the Poincaré map evaluated at the corresponding fixed point have its eigenvalues strictly within the unit circle.

The control design method experimentally implemented here begins with a parameterized family of continuous-time controllers that (i) induce a periodic orbit, and (ii) the orbit is invariant under the choice of controller parameters. The family of controllers can be constructed using a wide range of techniques [6], [10]–[15]. Properties of the Poincaré map and its first- and second-order derivatives are used to translate the problem of exponential stabilization of the periodic orbit

into a set of Bilinear Matrix Inequalities (BMIs). A BMI optimization problem is then set up to tune the parameters of the continuous-time controller so that the Jacobian of the Poincaré map has its eigenvalues in the unit circle. While simulations in [1], [2] indicated the promise of the method for stabilizing gaits in bipedal robots, here, experimental proof is provided.

In this paper, we employ the BMI optimization framework to systematically choose exponentially stabilizing virtual constraints for walking of MARLO, an underactuated bipedal robot. Virtual constraints are functional relations among generalized coordinates of a robot that are enforced asymptotically by feedback control; they are used to coordinate the links of the robot within a stride [3], [6], [16]–[23]. It has been shown that, for mechanical systems with more than one degree of underactuation, the stability of a walking gait depends on the choice of virtual constraints.
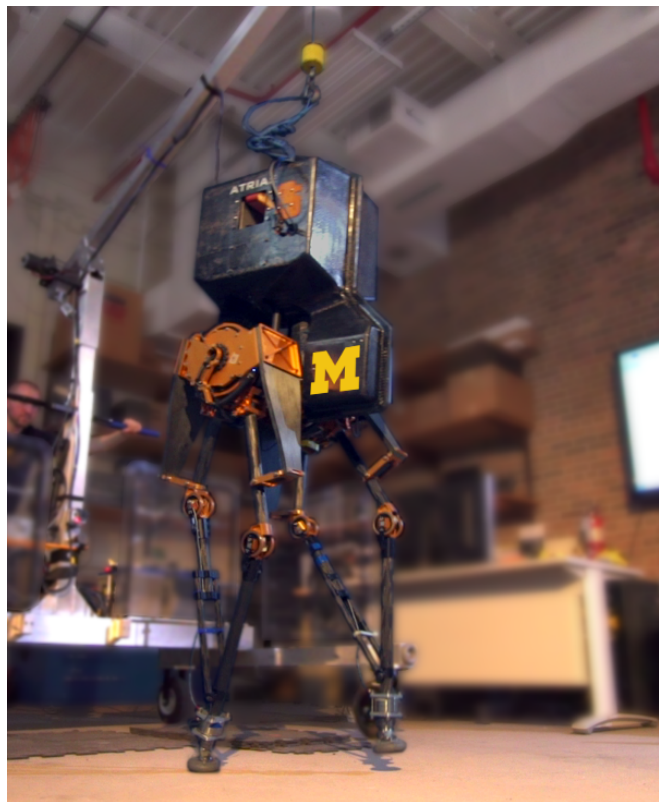
Fig. 1.   MARLO is one of three ATRIAS 2.1 robots designed and built by Jonathan Hurst at Oregon State University. Its point feet facilitate the study of dynamic bipedal locomotion. (Photo courtesty BTN LiveB1G)

[1]Department of Electrical Engineering and Computer Science, University of Michigan, Ann Arbor, MI 48109, USA {`bgbuss, griffb, grizzle`}`@umich.edu`
[2]Department of Mechanical Engineering, San Diego State University, San Diego, CA 92182, USA `kakbarihamed@mail.sdsu.edu`

Reference [24] used physical intuition to formulate a set of virtual constraints for walking of an underactuated 3D bipedal robot. However, the same intuition did not work to stabilize walking gaits of MARLO [3]. Subsequent work [25] presented preliminary walking experiments with MARLO in which an alternative heuristic was used to choose virtual constraints in the lateral plane, but it was very difficult to tune the controller. The current paper improves the virtual constraint design of [25] by employing the systematic BMI optimization algorithm to guarantee exponential stability of the walking gait.

The remainder of the paper is organized as follows. Section II presents the hybrid model of 3D walking. Section III presents a brief review of parameterized nonlinear state feedback laws and the systematic BMI optimization algorithm. Virtual constraints are presented in Section IV. Section V presents the experimental implementation of virtual constraints and stability analysis without the BMI algorithm. The BMI optimization for MARLO is presented in Section VI. Experimental results are provided in Section VII. Finally, Section VIII contains discussion and concluding remarks.

II. HYBRID MODEL OF 3D WALKING

MARLO is one of three ATRIAS-series bipedal robots designed at Oregon State University for robust, energetically efficient 3D walking; a complete description is given in [3]. The robot structure includes a torso and two identical legs terminating in point feet. Two motors drive each leg in the sagittal plane. In the frontal plane, one hip motor for each leg is connected to the body through fixed gear ratios. In total, the robot has 6 brushless DC motors.

Many of the key coordinates are shown in Fig. 2. In addition, three Euler angles, q_{zT} (yaw), q_{yT} (roll), and q_{xT} (pitch) specify the orientation of the torso link with respect to the world frame. Each sagittal-plane motor is connected to an upper link of the four-bar linkage legs through a 50:1 harmonic drive and a series spring. The angle of the output shaft of the harmonic drive is represented by the subscript "gr". In particular, we introduce q_{gr1R}, q_{gr2R}, q_{gr1L}, and q_{gr2L}. In addition, u_{1R}, u_{2R}, u_{1L} and u_{2L} denote the torques generated by the corresponding motor. The torques generated by the hip motors are denoted by u_{3R} and u_{3L}.

A vector of generalized coordinates is given by

$$(q_{zT}, q_{yT}, q_{xT}, q_{1R}, q_{2R}, q_{1L}, q_{2L},$$
$$q_{gr1R}, q_{gr2R}, q_{3R}, q_{gr1L}, q_{gr2L}, q_{3L}).$$

For the work presented here, MARLO was fitted with stiff springs which approximately constrain the link coordinates to be equal to the associated gear coordinates; thus we use the reduced vector of generalized coordinates

$$q := (q_{zT}, q_{yT}, q_{xT}, q_{gr1R}, q_{gr2R}, q_{3R}, q_{gr1L}, q_{gr2L}, q_{3L})^\top \in \mathcal{Q},$$

in which the first three components are unactuated, whereas the remaining six are actuated. Moreover, $\mathcal{Q} \subset \mathbb{R}^9$ denotes
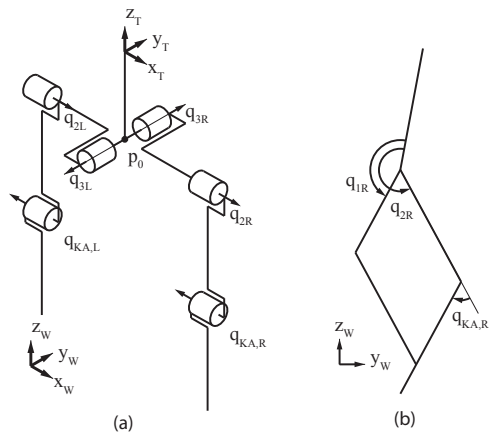
Fig. 2. Mechanical structure and coordinates for MARLO. (a) Conceptual diagram of rigid body model, with L and R denoting the left and right sides. (b) Each leg is physically realized by a four-bar linkage. The knee angle $q_{KA,R}$ is related to the angles of the upper links as $q_{KA,R} = q_{2R} - q_{1R}$.

the configuration manifold. The control inputs are given by the six-dimensional vector

$$u := (u_{1R}, u_{2R}, u_{3R}, u_{1L}, u_{2L}, u_{3L})^\top \in \mathcal{U},$$

where $\mathcal{U} \subset \mathbb{R}^6$ is the set of admissible control values.

The method of Lagrange is used to describe the evolution of the mechanical system in the standard form of an input-affine system $\dot{x} = f(x) + g(x)u$, in which $x := (q^\top, \dot{q}^\top)^\top \in \mathcal{X}$ represents the state vector and $\mathcal{X} := T\mathcal{Q}$ is the state manifold. The open-loop hybrid model of walking is then given by [3]

$$\Sigma : \begin{cases} \dot{x} = f(x) + g(x)\, u, & x^- \notin \mathcal{S} \\ x^+ = \Delta(x^-), & x^- \in \mathcal{S}, \end{cases} \quad (1)$$

in which $x^+ = \Delta(x^-)$ represents the instantaneous impact model. Furthermore, $\mathcal{S}$ is the switching manifold on which the solutions of the hybrid model (1) undergo an abrupt change in the velocity coordinates according to the impact map during walking on flat ground. In addition, x^- and x^+ denote the states of the system just before and after the impact event, respectively.

III. BMI OPTIMIZATION FOR STABILIZATION OF WALKING GAITS

This section briefly reviews the systematic optimization framework of [1], [2] involving BMIs and LMIs to exponentially stabilize periodic orbits for parameterized closed-loop models of bipedal locomotion. We consider a class of *parameterized nonlinear state feedback laws* as

$$u = \Gamma(x, \xi), \quad (2)$$

where $\Gamma(\cdot, \cdot)$ is at least C^2 and $\xi \in \Xi \subset \mathbb{R}^p$ represents the set of *tunable parameters* for some $p > 0$. We assume that by employing the smooth feedback law (2), there is a period-one orbit (i.e., waking gait) $\mathcal{O}$ for the closed-loop hybrid model which is (i) *transversal* to the switching manifold $\mathcal{S}$, and (ii) *invariant* under the choice of the controller parameters ξ.

The invariance property can be expressed as $\frac{\partial f^{\mathrm{cl}}}{\partial \xi}(x,\xi) = 0$ for all $(x,\xi) \in \overline{\mathcal{O}} \times \Xi$, where $f^{\mathrm{cl}}(x,\xi) := f(x) + g(x)\Gamma(x,\xi)$ and $\overline{\mathcal{O}}$ denotes the set closure of $\mathcal{O}$. The objective is then to tune the free parameters ξ to exponentially stabilize $\mathcal{O}$ for the closed-loop hybrid model. For this goal, we use the method of Poincaré sections.

The evolution of the system on the switching manifold $\mathcal{S}$ is given by the *parameterized Poincaré map*

$$x[k+1] = P(x[k], \xi), \qquad (3)$$

in which $x[k]$ denotes the system's state on the Poincaré section $\mathcal{S}$ and $k = 0, 1, \cdots$ denotes the step number. According to the invariance property, $x^* := \overline{\mathcal{O}} \cap \mathcal{S}$ is an *invariant fixed point* for P. Let $\xi^* \in \Xi$ be a nominal vector of controller parameters. The first-order approximation of the Jacobian of the Poincaré map $\frac{\partial P}{\partial x}(x^*, \xi)$ around $\xi = \xi^*$ is given by

$$\frac{\partial P}{\partial x}(x^*, \xi) \approx A_0 + \sum_{i=1}^{p} A_i \, \Delta\xi_i =: A(\Delta\xi), \qquad (4)$$

where $A_0 := \frac{\partial P}{\partial x}(x^*, \xi^*)$ is the *nominal Jacobian matrix*, the sequence $A_i := \frac{\partial^2 P}{\partial \xi_i \partial x}(x^*, \xi^*)$, $i = 1, \ldots, p$ denotes the *sensitivity matrices*, and $\Delta\xi := \xi - \xi^*$ is a small increment in controller parameters. Effective numerical approaches to calculate A_0 and A_i for $i = 1, \cdots, p$ are presented in [2].

A BMI optimization problem can then be formulated as

$$\min_{W, \Delta\xi, \mu, \eta} -w\,\mu + \eta \qquad (5)$$

$$\text{s.t.} \quad \begin{bmatrix} W & A(\Delta\xi)W \\ \star & (1-\mu)\,W \end{bmatrix} > 0 \qquad (6)$$

$$\begin{bmatrix} I & \Delta\xi \\ \star & \eta \end{bmatrix} > 0 \qquad (7)$$

$$\mu > 0, \qquad (8)$$

in which $W = W^\top > 0$ and $\mu > 0$ are decision variables introduced to express stability of $A(\Delta\xi)$ in terms of the BMI (6). Indeed, by Schur's lemma, $\sqrt{1-\mu}$ is an upper bound for the spectral radius of $A(\Delta\xi)$ when (6) and (8) are satisfied. Similarly, (7) implies that η is an upper bound on $\|\Delta\xi\|_2^2$. The optimization tries to minimize a linear combination of μ and η; adjusting the weight w affects the tradeoff between improving the convergence rate (i.e., minimizing $\sqrt{1-\mu}$) and ensuring that $A(\Delta\xi)$ remains a reasonable approximation of $\frac{\partial P}{\partial x}(x^*, \xi)$ (i.e., minimizing $\|\Delta\xi\|_2$).

IV. VIRTUAL CONSTRAINTS FOR 3D WALKING

Virtual constraints are relations on the state variables of the robot's model that are achieved through the action of actuators and feedback control instead of physical contact forces. They are called *virtual* because they can be reprogrammed on the fly without modifying any physical connections among the links of the robot or its environment. Virtual constraints can be used to synchronize the evolution of a robot's links to create periodic motion, such as walking [3], [6], [16]–[23]. They are implemented as output functions which are in turn regulated to zero by feedback laws.

A. Parameterized Virtual Constraints

In this paper, we consider *parameterized holonomic virtual constraints* as follows

$$\begin{aligned} y(x,\xi) &:= h_0(q,\xi) - h_{\mathrm{d}}(\theta(q),\xi) \\ &:= H(\xi)\,(q - q_{\mathrm{d}}(\theta(q))), \end{aligned} \qquad (9)$$

where $h_0(q,\xi) := H(\xi)\,q$ represents the set of *controlled variables* and $h_{\mathrm{d}}(\theta,\xi) := H(\xi)\,q_{\mathrm{d}}(\theta)$ denotes the *desired evolution* of the controlled variables along the desired gait $\mathcal{O}$. In addition, $H(\xi) \in \mathbb{R}^{6 \times 9}$ is an *output matrix* to be determined and $q_{\mathrm{d}}(\theta)$ represents the desired evolution of the generalized coordinates on the desired walking gait. The function $\theta(q)$ denotes the *gait phasing variable* that is a strictly monotonic (increasing or decreasing) quantity along the orbit $\mathcal{O}$. In particular, θ plays the role of time, which is a key to obtaining time-invariant feedback laws. By designing the output $y(x,\xi)$ to have vector relattive degree $(2, \cdots, 2)$ with respect to u, an I/O linearizing controller of the form

$$\Gamma(x,\xi) = -\left(\mathrm{L}_g \mathrm{L}_f y\right)^{-1} \left(\mathrm{L}_f^2 y + \frac{K_D}{\varepsilon}\,\mathrm{L}_f y + \frac{K_P}{\varepsilon^2}\,y\right), \qquad (10)$$

where $K_D, K_P, \varepsilon > 0$, can be used to zero the outputs represented by the virtual constraints. It can be shown that the feedback law of (10) satisfies the invariance assumption of Section III and hence, we can employ the BMI optimization framework to properly choose the output matrix $H(\xi)$ to guarantee the asymptotic stability of the walking gait $\mathcal{O}$. For later purposes, we define the *parameterized zero dynamics manifold* corresponding to the output y as

$$\mathcal{Z}(\xi) := \{x \in \mathcal{X} \,|\, y(x,\xi) = \mathrm{L}_f y(x,\xi) = 0\}, \qquad (11)$$

on which the output y is identically zero. We also remark that the I/O linearizing feedback law (10) renders the zero dynamics manifold $\mathcal{Z}$ forward invariant and attractive.

B. Nominal Controlled Variables

This section presents a nominal set of controlled variables $(H(\xi^*)\,q)$ for MARLO around which the BMI optimization of (5) will be solved. The nominal controlled variables in the sagittal plane are selected as the swing and stance leg and knee angles [3]. For each leg, the *virtual leg* is defined as the the virtual line connecting the leg end to the corresponding hip joint. The leg angle is then defined as the angle of the virtual leg with respect to the torso link. As stated in Sect. I, the choice of controlled variables in the lateral plane is critical for stability. Intuition and analysis both suggest that stability is unlikely to be achieved when virtual constraints ignore lateral motion of the robot [24], [3] [25]. For the lateral plane, two controlled variables are chosen in this paper. The first one is taken as the stance hip angle, whereas the second one is defined for the swing hip angle based on the concept of SIMBICON of [26]. Taken together, the vector of nominal controlled variables during the right stance phase

becomes

$$H(\xi^*)\,q = \begin{bmatrix} \frac{1}{2}\left(q_{\mathrm{gr1R}} + q_{\mathrm{gr2R}}\right) \\ \frac{1}{2}\left(q_{\mathrm{gr1L}} + q_{\mathrm{gr2L}}\right) \\ q_{\mathrm{gr2R}} - q_{\mathrm{gr1R}} \\ q_{\mathrm{gr2L}} - q_{\mathrm{gr1L}} \\ q_{\mathrm{3R}} \\ q_{\mathrm{3L}} - (1 + c_p)q_{y\mathrm{T}} - c_p q_{\mathrm{3R}} \end{bmatrix}, \qquad (12)$$

in which the first two components represent the stance and swing leg angles, and the third and fourth components denote the stance and swing knee angles, respectively. The fifth component is the stance (i.e., right) leg hip angle. Finally, the sixth component represents the linearized version of the SIMBICON-based controlled variable introduced in [25], where $c_p := 0.85$ is a constant. While the SIMBICON-based virtual constraint effectively stabilized the walking gait in [25], tuning the parameters of the the output was a delicate task. Indeed, the collective analytical and experimental results of [24], [3] and [25] motivated the development of the BMI optimization method for systematically selecting virtual constraints.

The gait phasing variable is defined as the angle of the hip with respect to the stance foot. In addition, the periodic walking motion $\mathcal{O}$ is designed using the motion planning algorithm of [3].

V. EXPERIMENTAL IMPLEMENTATION OF VIRTUAL CONSTRAINTS AND STABILITY ANALYSIS

This section presents and analyzes several variations on the I/O linearizing control law which will be used in experiments.

A. Feedback Linearization

Employing the input-output linearizing feedback law in simulation permits us to study the effects of different choices of virtual constraints on the stability of an orbit. Because, when this feedback law is combined with the event-based updates described below, the zero dynamics manifolds become hybrid invariant, we can isolate the stabilizing effect of the choice of virtual constraints from the effect of PD control.

B. Event-Based Update

Following the approach of [27] to achieve hybrid invariance of the zero dynamics manifold, we first parameterize the outputs with the second set of parameters α, referred to as the hybrid invariance parameters, as follows

$$y(x, \xi, \alpha) := h_0(q, \xi) - h_{\mathrm{d}}(\theta(q), \xi, \alpha). \qquad (13)$$

Then we employ an event-based law to update α to zero the output function $y(x, \xi, \alpha)$ and its time-derivative at the beginning of the step. The parameters α also remain constant until the next impact. Further details on this approach can be found in [27].

C. PD + Feedforward

Feedback linearization can be sensitive to parametric uncertainty in the model. For this reason we will only use (10) for gait design and stability analysis. Following [28], we make use of a modified version of (10) for experimental implementation. The modification consists of substituting regressed torques for the nominal torque on the orbit, i.e., u^*, and a *constant* matrix T for the decoupling matrix $\mathrm{L}_g \mathrm{L}_f y$. The nominal (i.e., feedforward) torque is determined from the simulation model by regressing the torques along the periodic orbit as 5th order Bézier polynomials in the *normalized gait phasing variable* s. Thus the feedback law used is given by

$$u_{\exp} = u^*(s) - T^{-1}\left(\frac{K_D}{\varepsilon}\dot{y} + \frac{K_P}{\varepsilon^2}y\right). \qquad (14)$$

It can be shown that the modified feedback law of (14) satisfies the invariance property of the orbit with respect to controller parameters ξ as stated in Section III.

D. Stability Analysis

To evaluate the stability of the designed gait under various choices of feedback we compute the linearized Poincaré maps of the corresponding closed-loop systems. Jacobians are estimated by symmetric differences with a uniform step size of 10^{-4} radians. Feedback gains K_P, K_D, and ε were chosen based on walking experiments.

Feedback linearization with event-based update. For this feedback law the dominant eigenvalues of the linearized Poincaré map for the closed-loop system are $\{-1.84, -1, 0.75, -0.49, 0.43\}$. The eigenvalue -1 corresponds to yaw, and is expected as neither the robot dynamics nor the feedback controller depend on yaw [29, Prop. 4], [30, Thm. 3].

Feedback linearization without event-based update. For this feedback law the dominant eigenvalues are $\{-1.64, -1, 0.75, -0.46, 0.35\}$. This feedback law will be used in conjunction with BMI optimization to determine how the virtual constraints should be modified to achieve exponential stability of the orbit.

PD + feedforward with event-based update. For this feedback law the dominant eigenvalues are $\{-1.99, -1, 0.72, -0.54, 0.24\}$. One practical motivation for using event-based updates is to reduce the magnitude of discontinuities in the torque at step transitions.

PD + feedforward without event-based update. Disabling the event-based updates leads to a simpler control law which nevertheless approximately enforces the virtual constraints. The dominant eigenvalues in this case are $\{-1.77, -1, 0.74, -0.54, 0.23\}$.

VI. BMI OPTIMIZATION OF CONTROLLED VARIABLES

This section employs the BMI optimization algorithm of Section III as a systematic means to search for a set of controlled variables to exponentially stabilize the walking gait for the closed-loop model of the robot.

A. Parametrization of the Constraints

For the experiments reported here, we consider the parameterized virtual constraints of (9) with H selected to allow each virtual constraint to depend on the torso roll angle. The motivation for this is based on [24], [3] and [25], where various heuristics used the roll angle to achieve "stability in the lateral motion of the robot". We therefore have

$$
H(\xi) = \begin{bmatrix}
0 & \xi_1 & 0 & \frac{1}{2} & \frac{1}{2} & 0 & 0 & 0 & 0 \\
0 & \xi_2 & 0 & 0 & 0 & 0 & \frac{1}{2} & \frac{1}{2} & 0 \\
0 & \xi_3 & 0 & -1 & 1 & 0 & 0 & 0 & 0 \\
0 & \xi_4 & 0 & 0 & 0 & 0 & -1 & 1 & 0 \\
0 & \xi_5 & 0 & 0 & 0 & 1 & 0 & 0 & 0 \\
0 & \xi_6 - (1 + c_p) & 0 & 0 & 0 & -c_p & 0 & 0 & 1
\end{bmatrix}.
$$
(15)

The nominal controlled coordinates in (15) are simply $H(\xi^*)q$, where $\xi^* = 0$ is the nominal choice of parameters.

Because we have chosen not to make the virtual constraints yaw-dependent, the linearized Poincaré map of the closed-loop system will have an eigenvalue of -1 for all values of ξ. Thus, to proceed with an optimization "modulo yaw", we eliminate the yaw coordinate by a simple projection. Specifically, after computing the Jacobian $A_0 = \frac{\partial P}{\partial x}(x_f^*, \xi^*)$ of the corresponding Poincaré map and the sensitivities A_i, $i = 1, \ldots, 6$ of A_0 with respect to perturbations in ξ_i, we remove the first row and column of each. The resulting matrices are assembled into the affine matrix function $A(\Delta\xi) = A_0 + \sum_{i=1}^{6} A_i \Delta\xi_i$ comprising the model data needed for the BMI optimization problem (5). Using PENBMI and YALMIP this optimization problem is solved with the cost weight $w = 10$.

B. Computational Results

The optimal perturbation of ξ is found to be $\Delta\xi = (-0.26, 0.20, 0.30, -0.23, -0.06, 0.24)$, and the corresponding spectral radius of $A(\Delta\xi)$ is 0.28.

When the revised virtual constraints are used in each of the closed-loop systems described in Section V-D, the eigenvalues of the linearized Poincaré map are: Feedback linearization with event-based update: $\{-1, -0.68, 0.68, -0.32, 0.08\}$; Feedback linearization without event-based update: $\{-1, 0.58, -0.42, -0.42, 0.32\}$; PD + feedforward with event-based update: $\{-1, -0.34, -0.34, 0.56, -0.39\}$; PD + feedforward without event-based update: $\{-1, -0.34, -0.34, 0.53, -0.04\}$. As before, the eigenvalue -1 corresponds to yaw.

We see that the revised virtual constraints stabilize the orbit for the closed-loop system with any of the control laws considered.

VII. EXPERIMENTAL EVALUATION

A. Method

The controller design based on BMI-optimized constraints was evaluated on MARLO and compared to the controller based on the nominal virtual constraints. Experiments were performed on flat ground in the laboratory, where MARLO can walk approximately 7-8 meters during a single experiment. Power was supplied by an off-board battery bank carried on a mobile gantry. The gantry is designed to catch the robot when power is cut at the end of an experiment, or in the event of an early failure. It does not support the robot or provide any stabilization during the walking experiments.

In each experiment the control software executes a gait initiation sequence as follows:

1) **Posing.** The robot is placed in its initial pose and then lowered from the gantry to the ground where it begins supporting its own weight. Because the toroidal feet are not large enough to achieve static balance, an experimenter manually stabilizes the robot's COM over the feet. The control software waits for the experimenter to release the robot before entering the Injection phase. Release is detected by comparing the pitch rate to a pre-specified threshold of -3 degrees per second.

2) **Injection.** When the pitch rate crosses the threshold, the controller initiates a lateral rocking motion away from the left leg by rapidly extending the left knee 5 degrees from the posing configuration.

3) **Transition.** The software then enters the Transition phase, in which it initiates a short first step to accelerate the robot forward. The transition step employs hand-modified virtual constraints originally based on an optimization [31].

4) **Walking.** After a single transition step, the walking virtual constraints are activated and remain in use for the duration of the experiment. Swing leg impact is detected using the knee angle spring deflection on the swing and stance legs. During the first five steps of the Walking phase, the torso is offset several degrees forward to help the robot gain speed.

Prior to the experiments reported here, a series of experiments were run in which the virtual constraints were minimally adjusted to achieve walking. This is necessary due to current discrepancies between the model and the robot. The swing knee angle virtual constraint, in particular, required the most tuning. It is hypothesized that this is due to a combination of stiction in the harmonic drives and limitations in peak motor torque. The swing knee angle feedforward torque was also adjusted by hand to improve tracking. These modifications caused the actual trajectory followed by the robot to more closely match the originally designed trajectory.

In each experiment the robot was allowed to walk until: 1) the robot approached the perimeter of the walking area; 2) the state of the robot left a (conservative) safe operating region; or 3) an experimenter cut motor power. The last of these occurred twice; in both cases the robot lost forward momentum and appeared to be on the verge of falling when the power was cut.

B. Results

Eighteen experiments were performed as reported in Table I. The superiority of the BMI-optimized outputs in stabilizing the gait is evident. Ten of the experiments with event-based updates enabled are described here: five using the nominal outputs, and five using the BMI-optimized outputs.

ID[a]	Controlled coordinates	Event-based update	Total steps	Reason ended
N1	nominal	enabled	14	power cut
B1	optimized	enabled	19	end of lab
B2	optimized	enabled	14	end of lab
N2	nominal	enabled	11	power cut
B3	optimized	enabled	4	power cut
N3	nominal	enabled	10	power cut[b]
B4	optimized	enabled	15	end of lab
N4	nominal	enabled	4	power cut
B5	optimized	enabled	13	end of lab
N5	nominal	enabled	3	power cut
B6	optimized	disabled	15	end of lab
B7	optimized	disabled	20	end of lab
N6	nominal	disabled	6	power cut
N7	nominal	disabled	14	power cut
B8	optimized	disabled	19	end of lab
B9	optimized	disabled	19	end of lab

[a] Experiments are listed in the order they were performed. Additional runs (including runs for filming by BTN LiveB1G) were performed between some of the experiments listed above.
[b] Safety stop preceded by external disturbance from the safety cable.

See [32] for details and additional experiments with event-based updates disabled.

In four of the five experiments using BMI-optimized outputs, the robot reached the perimeter of the walking area in the lab. A video of the experiments is available on YouTube [33]. Because yaw is not directly regulated, the robot tended to turn gradually while walking. There was less yaw motion when using the nominal outputs.

Figure 3 shows the motion of the torso. Here the gradual turning is evident. The average yaw rate was around -9.8 degrees per second with the nominal outputs and -11.0 degrees per second with the optimized outputs. The torso pitch oscillates with each step. The amplitude of the oscillation (between 6–10 degrees peak to peak) is somewhat larger than in simulation (5.5 degrees peak to peak).

The most notable difference in the torso motion is in the roll angle. From the simulation, we expect the peak-to-peak torso roll to be about 4.4 degrees. The nominal controller fails to effectively stabilize the torso roll. On the other hand, after a transient following gait initiation, the optimized controller brings the torso oscillation to between 4 and 6 degrees peak to peak.

The stabilizing effect is further evident in the motion of the COM. Figure 4 shows the linearized COM position with respect to the right foot.[1] From these plots we see that the relative motion of the COM in the sagittal plane is very

[1] Computed as $\hat{p}_{\text{COM}}(q) = J_{\text{COM}}(q - q_0)$ where $J_{\text{COM}} = \frac{\partial p_{\text{COM}}^{R}}{\partial q}(q)\big|_{q=q_0}$ is a constant matrix, $p_{\text{COM}}^{R}(q)$ is the position of the COM with respect to the right leg, and q_0 is a symmetric, upright nominal configuration.
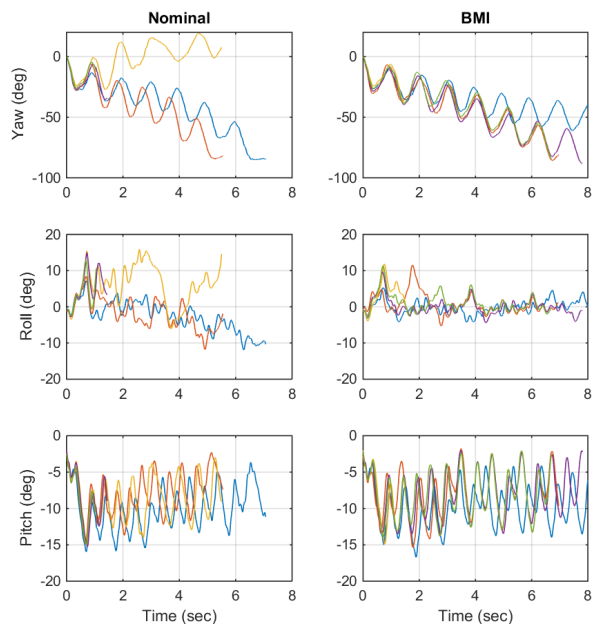
Fig. 3. Torso Euler angles with event-based updates enabled. The plots compare the results from ten walking experiments, five of which used the nominal outputs (left column; experiments N1, N2, N3, N4, N5) and five of which used the optimized outputs (right column; experiments B1, B2, B3, B4, B5).
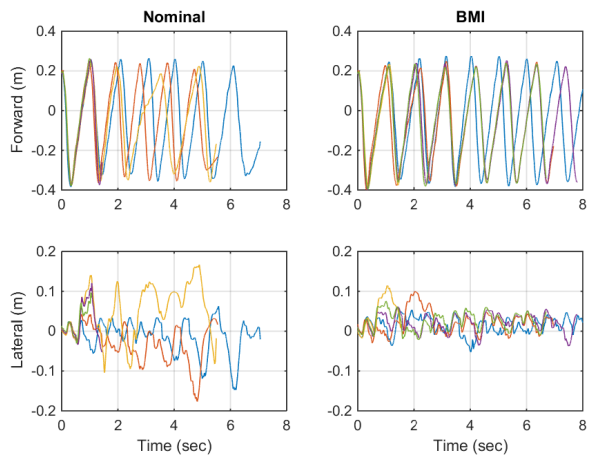
Fig. 4. Linearized position of the COM with event-based updates enabled. The plots compare the results from ten walking experiments, five of which used the nominal outputs (left column; experiments N1, N2, N3, N4, N5) and five of which used the BMI-optimized outputs (right column; experiments B1, B2, B3, B4, B5).
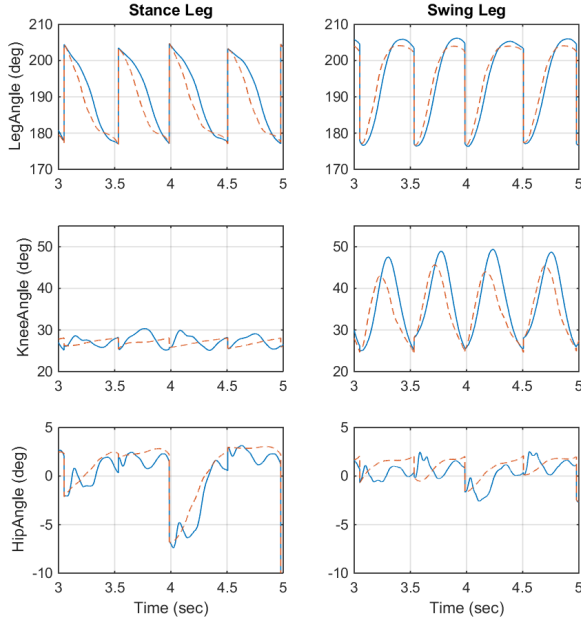
Fig. 5. Tracking of desired evolutions when using the nominal outputs. The data are from experiment N1, and are representative of the other experiments. The dashed lines show the desired evolution of the controlled variables, and the solid lines represent their actual evolution.

Fig. 6. Tracking of desired evolutions when using the optimized outputs. The data are from experiment B1, and are representative of the other experiments. The dashed lines show the desired evolution of the controlled variables, and the solid lines represent their actual evolution.

similar for all four controllers tested. However, the motion of the COM in the lateral plane is quite exaggerated when the nominal outputs are used. When the optimized outputs are used, the COM is maintained very close to the nominal position.

The low-level joint tracking errors were generally comparable. Figures 5 and 6 compare the desired evolutions with the actual trajectories of the controlled coordinates for experiments N1 and B1, respectively.

VIII. DISCUSSION AND CONCLUSIONS

The experimental results indicate that the virtual constraints designed on the basis of the BMI optimization algorithm are more effective at lateral stabilization than the nominal constraints. The robot walked farther, more consistently, and with less torso and COM oscillation in the lateral plane with the optimized virtual constraints compared to the nominal virtual constraints. A potential physical mechanism by which this is achieved is given next. In the lateral plane, the optimal perturbation $\Delta \xi$ primarily affects the swing hip angle. It effectively reduces the SIMBICON gain c_p, yielding less swing hip abduction in response to the robot rolling to the inside of the stance foot. This in turn will lead the swing foot to impact the ground earlier, reducing the magnitude of step-to-step oscillations in the lateral plane. In the sagittal plane, increased roll motion toward the swing leg causes the stance leg to shorten and swing leg to lengthen, terminating the step earlier in the gait.

While the results of these experiments are promising, limitations are acknowledged. In particular, due to the relatively short walking distance available in the lab, it is difficult to separate the effects of initial conditions from the long-term behavior of the robot under a particular controller. Variability in the initial conditions may be caused by small differences in how the robot is posed, how the robot initially falls forward, and where it takes its first step during the injection phase. While the magnitudes of these differences should be similar for each of the controllers, and one of them did yield consistently more steps than the other, it is nevertheless important to repeat the experiments outdoors with much longer runs. Recent work has shown how to include disturbance rejection directly into the design problem for the periodic orbit [34], [35]. In addition, the BMI optimization algorithm presented in [2] also allows for disturbance rejection metrics to be incorporated into the problem formulation, allowing one to search for stabilizing solutions with enhanced disturbance rejection capabilities. Each of these methods will be explored on the robot.

1231171.

REFERENCES

[1] K. Akbari Hamed, B. G. Buss, and J. W. Grizzle, "Continuous-time controllers for stabilizing periodic orbits of hybrid systems: Application to an underactuated 3d bipedal robot," in *Decision and Control (CDC), 2014 IEEE 53rd Annual Conference on*, Dec 2014, pp. 1507–1513.

[2] ——, "Exponentially stabilizing continuous-time controllers for periodic orbits of hybrid systems: Application to bipedal locomotion with ground height variations," *The International Journal of Robotics Research*, published online, August 2015.

[3] A. Ramezani, J. W. Hurst, K. Akbari Hamed, and J. W. Grizzle, "Performance Analysis and Feedback Control of ATRIAS, A Three-Dimensional Bipedal Robot," *Journal of Dynamic Systems, Measurement, and Control*, no. 2, Dec.

[4] J. Grimes and J. Hurst, "The design of ATRIAS 1.0 a unique monopod, hopping robot," *Climbing and walking Robots and the Support Technologies for Mobile Machines, International Conference on*, 2012.

[5] "DARPA Robotics Challenge," http://www.theroboticschallenge.org/, 2015.

[6] J. W. Grizzle, C. Chevallereau, R. W. Sinnet, and A. D. Ames, "Models, feedback control, and open problems of 3d bipedal robotic walking," *Automatica*, vol. 50, no. 8, pp. 1955–1988, 2014.

[7] V. Arnold, *Mathematical Methods of Classical Mechanics*. New York NY Berlin Paris : Springer, 1989, translated by : Karen Vogtmann and Alan D. Weinstein.

[8] W. M. Haddad, V. S. Chellaboina, and S. G. Nersesov, *Impulsive and Hybrid Dynamical Systems: Stability, Dissipativity, and Control*. Princeton, NJ: Princeton University Press, 2006.

[9] C. O. Saglam, A. R. Teel, and K. Byl, "Lyapunov-based versus poincare map analysis of the rimless wheel," in *Decision and Control (CDC), 2014 IEEE 53rd Annual Conference on*. IEEE, 2014, pp. 1514–1520.

[10] K. Byl and R. Tedrake, "Metastable walking machines," *The International Journal of Robotics Research*, vol. 28, no. 8, pp. 1040–1064, 2009.

[11] I. R. Manchester, U. Mettin, F. Iida, and R. Tedrake, "Stable dynamic walking over uneven terrain," *The International Journal of Robotics Research*, vol. 30, no. 3, pp. 265–279, 2011. [Online]. Available: http://ijr.sagepub.com/content/30/3/265.abstract

[12] H. Dai and R. Tedrake, "L2-gain optimization for robust bipedal walking on unknown terrain," in *Robotics and Automation (ICRA), 2013 IEEE International Conference on*, 2013.

[13] A. S. Shiriaev, L. B. Freidovich, and I. R. Manchester, "Can we make a robot ballerina perform a pirouette? orbital stabilization of periodic motions of underactuated mechanical systems," *Annual Reviews in Control*, vol. 32, no. 2, pp. 200–211, 2008.

[14] A. S. Shiriaev and L. B. Freidovich, "Transverse linearization for impulsive mechanical systems with one passive link," *Automatic Control, IEEE Transactions on*, vol. 54, no. 12, pp. 2882–2888, 2009.

[15] A. D. Ames, "Human-inspired control of bipedal walking robots," *Automatic Control, IEEE Transactions on*, vol. 59, no. 5, pp. 1115–1130, 2014.

[16] L. Freidovich, U. Mettin, A. Shiriaev, and M. Spong, "A passive 2-DOF walker: Hunting for gaits using virtual holonomic constraints," *Robotics, IEEE Transactions on*, vol. 25, no. 5, pp. 1202–1208, Oct 2009.

[17] A. D. Ames, E. A. Cousineau, and M. J. Powell, "Dynamically stable robotic walking with NAO via human-inspired hybrid zero dynamics," in *Hybrid Systems, Computation and Control (HSCC)*, Philadelphia, April 2012.

[18] J. Lack, M. Powell, and A. Ames, "Planar multi-contact bipedal walking using hybrid zero dynamics," in *Robotics and Automation, IEEE International Conference on*, May 2014, pp. 2582–2588.

[19] R. Gregg and J. Sensinger, "Towards biomimetic virtual constraint control of a powered prosthetic leg," *Control Systems Technology, IEEE Transactions on*, vol. 22, no. 1, pp. 246–254, Jan 2014.

[20] R. Gregg, T. Lenzi, L. Hargrove, and J. Sensinger, "Virtual constraint control of a powered prosthetic leg: From simulation to experiments with transfemoral amputees," *Robotics, IEEE Transactions on*, vol. 30, no. 6, pp. 1455–1471, Dec 2014.

[21] C. Chevallereau, G. Abba, Y. Aoustin, F. Plestan, E. Westervelt, C. Canudas-de Wit, and J. Grizzle, "Rabbit: a testbed for advanced control theory," *Control Systems, IEEE*, vol. 23, no. 5, pp. 57–79, Oct 2003.

[22] M. Maggiore and L. Consolini, "Virtual holonomic constraints for Euler Lagrange systems," *Automatic Control, IEEE Transactions on*, vol. 58, no. 4, pp. 1001–1008, April 2013.

[23] A. Martin, D. Post, and J. Schmiedeler, "The effects of foot geometric properties on the gait of planar bipeds walking under HZD-based control," *The International Journal of Robotics Research*, vol. 33, no. 12, pp. 1530–1543, 2014.

[24] C. Chevallereau, J. Grizzle, and C. Shih, "Asymptotically stable walking of a five-link underactuated 3D bipedal robot," *IEEE Transactions on Robotics*, vol. 25, no. 1, pp. 37–50, February 2009.

[25] B. Buss, A. Ramezani, K. Hamed, B. Griffin, K. Galloway, and J. Grizzle, "Preliminary walking experiments with underactuated 3d bipedal robot marlo," in *Intelligent Robots and Systems (IROS 2014), 2014 IEEE/RSJ International Conference on*, Sept 2014, pp. 2529–2536.

[26] K. Yin, K. Loken, and M. van de Panne, "SIMBICON: Simple biped locomotion control," *ACM Transactions on Graphics*, vol. 26, no. 3, 2007. [Online]. Available: http://doi.acm.org/10.1145/1276377.1276509

[27] B. Morris and J. W. Grizzle, "Hybrid invariant manifolds in systems with impulse effects with application to periodic locomotion in bipedal robots," *IEEE Transactions on Automatic Control*, vol. 54, no. 8, pp. 1751–1764, August 2009.

[28] K. Sreenath, H. Park, I. Poulakakis, and J. Grizzle, "A compliant hybrid zero dynamics controller for stable, efficient and fast bipedal walking on MABEL," *International Journal of Robotics Research*, vol. 30(9), pp. 1170–1193, 2011.

[29] C.-L. Shih, J. Grizzle, and C. Chevallereau, "From Stable Walking to Steering of a 3D Bipedal Robot with Passive Point Feet," *Robotica*, vol. 30, no. 07, pp. 1119–1130, December 2012.

[30] K. Akbari Hamed and J. W. Grizzle, "Event-based stabilization of periodic orbits for underactuated 3-d bipedal robots with left-right symmetry," *Robotics, IEEE Transactions on*, vol. 30, no. 2, pp. 365–381, 2014.

[31] A. Ramezani, "Feedback control design for MARLO, a 3D-bipedal robot," PhD Thesis, University of Michigan, 2013.

[32] B. G. Buss, "Systematic controller design for dynamic 3d bipedal robot walking," Ph.D. dissertation, University of Michigan, 2015.

[33] Dynamic Leg Locomotion YouTube Channel. (2015) MARLO: Dynamic 3D walking based on HZD gait design and BMI constraint selection, https://www.youtube.com/watch?v=5ms5DtPNwHo.

[34] H. Dai and R. Tedrake, "Optimizing robust limit cycles for legged locomotion on unknown terrain," in *Decision and Control (CDC), 2012 IEEE 51st Annual Conference on*, 2012, pp. 1207–1213.

[35] B. Griffin and J. Grizzle, "Walking gait optimization for accommodation of unknown terrain height variations," in *American Control Conference (ACC), 2015*, July 2015, pp. 4810–4817.